Finite-size effects in antiferroelectric $PbZrO_3$ nanoparticles

1997 J. Phys.: Condens. Matter 9 8135

(http://iopscience.iop.org/0953-8984/9/38/017)

J. Phys.: Condens. Matter **9** (1997) 8135–8145. Printed in the UK PII: S0953-8984(97)83387-5

Finite-size effects in antiferroelectric $PbZrO_3$ nanoparticles

Soma Chattopadhyay, Pushan Ayyub†, V R Palkar, A V Gurjar, R M Wankar and Manu Multani

Materials Research Group, Tata Institute of Fundamental Research, Homi Bhabha Road, Mumbai 400 005, India

Received 14 April 1997, in final form 19 June 1997

Abstract. We study the size dependence of the antiferroelectric-to-paraelectric phase transition in ultrafine particles of $PbZrO_3$ (with x-ray domain size down to ≈30 nm) prepared by the sol–gel method. The phase transition was investigated by means of dielectric and thermal measurements. The nature of the particle size dependence of various properties of antiferroelectric $PbZrO_3$ was found to be generally similar to that of typical 'displacive' ferroelectrics such as $PbTiO_3$ and $BaTiO_3$. In both cases, a size-induced structural distortion towards the high-symmetry paraelectric phase appears to dictate the behaviour of the nanoparticulate system. Nanoparticles of 'order–disorder' systems such as $NaNO_2$ behave in a markedly different manner. With decreasing particle size, we observe an increasing deviation of the dielectric response from the Curie–Weiss behaviour. Certain physical situations that may lead to the observed smearing out of the transition in nanoparticles of $PbZrO_3$ and $PbTiO_3$ are discussed.

1. Introduction

Finite-size effects in ferroelectric materials have been investigated for a long time [1, 2], though most earlier studies were restricted to sintered ceramic samples with a grain size in the micrometre range [3, 4]. The rapid development of several advanced synthetic techniques such as the sol–gel, co-precipitation, spray-pyrolysis, aerosol, microemulsion, sputtering, evaporation, and laser ablation has made it possible to study different compounds in the form of phase-pure, ultrafine particles with a relatively narrow size distribution. There is now a strong motivation for the study of finite-size effects in ferroelectric and antiferroelectric systems in view of their current and potential applications as sensors, microelectromechanical devices and memory elements [5].

Using the phenomenological Landau–Devonshire theory, Zhong *et al* [6] have shown that the ferroelectric critical temperature T_C should decrease with decreasing size, ultimately leading to a size-driven phase transition from the ferroelectric to the paraelectric phase. This appears to agree with the size dependence of T_C in sub-micron $PbTiO_3$ particles observed in measurements of the specific heat [7] and Raman mode softening [8]. A similar result was also obtained for $BaTiO_3$ [9]. In a recent study of the ferroelectric phase transition in nanocrystalline $PbTiO_3$ using dielectric, thermal and structural measurements [10], it was established that with decreasing particle size: (1) there is a monotonic decrease in the ferroelectric T_C, (2) the crystallographic unit cell tends towards higher symmetry (i.e. tetragonal distortion, $c/a \rightarrow 1$), (3) the value of the peak dielectric constant (ε_{max})

† Author to whom any correspondence should be addressed.

0953-8984/97/388135+11$19.50

decreases, and (4) the ferroelectric transition deviates from the Curie–Weiss behaviour and becomes increasingly diffuse.

Interestingly, in *sintered* ferroelectric samples with a grain size in the 1–5 μm range, T_C shows a small *increase* with decreasing grain size. This has been ascribed to the effects of the space charge in the grain boundaries [11] and the stress system produced on cooling the system through T_C [12].

However, there does not appear to be any similarly detailed study of finite-size effects in any of the analogous antiferroelectric compounds. Here we report a study of size effects in nanocrystalline $PbZrO_3$, which is one of the best-known antiferroelectric compounds, besides being a constituent of the technologically important piezoelectric compound $Pb(Ti_{1-x}Zr_x)O_3$ (PZT). Antiferroelectrics are characterized by the existence of an antiparallel-ordered array of local dipoles with equal and opposite sublattice dipole moments, which results in a net zero polarization in the crystal. Ideally, they show no dielectric hysteresis and undergo a transition to a paraelectric phase of higher symmetry at T_C, where there is a sharp anomaly in the dielectric response. Some antiferroelectrics transform to a ferroelectric phase when heated (to just below T_C) or subjected to an electric field. The difference in the free energy between such antiferroelectric and ferroelectric phases of a material is usually quite small.

$PbZrO_3$ has an orthorhombic structure at room temperature ($a = 0.824$ nm, $b = 1.176$ nm, $c = 0.588$ nm) with the crystallographic unit cell containing eight formula units. This structure is derived from a cubic perovskite prototype (the high-temperature paraelectric phase) by antiparallel displacements of the Pb ions along one of the original [110] directions—which becomes the a-axis of the orthorhombic phase. In order to compare the unit cells of the paraelectric and the ferroelectric phases, it is often convenient to ignore the displacements of the Pb ions. This leads to a pseudo-tetragonal unit cell in the ordered phase, whose lattice constants (a_T, c_T) are related to the actual orthorhombic unit cell (a, b, c) as follows:

$$a_T = a/\sqrt{2} \qquad c_T = c/2.$$

$PbZrO_3$ shows a strong dielectric anomaly at $T_C \approx 230\ ^\circ$C and transforms to the cubic paraelectric phase above T_C. It has recently been suggested that, even at room temperature, $PbZrO_3$ possesses a weak ferroelectricity along the c-direction, coexisting with the antiferroelectric order in the a–b plane [13].

We have prepared ultrafine particles (down to about 30 nm) of $PbZrO_3$ by the sol–gel method. The average particle size was calculated from x-ray diffraction (XRD) line broadening and was compared to the sizes obtained from specific surface area measurement and scanning electron microscopy. The paraelectric phase transition in samples with different average sizes was studied by differential scanning calorimetry (DSC) and on the basis of the temperature dependence of the dielectric response function.

While nanoparticles of *displacive* systems such as $PbZrO_3$ and $PbTiO_3$ were found to show certain essential similarities, their behaviour differs from that of a typical *order–disorder* system such as $NaNO_2$. Conventionally, a system is termed 'displacive' when the elementary dipoles strictly vanish in the paraelectric phase, and 'order–disorder' when they are non-vanishing but thermally average out to zero in the paraelectric phase. It is also possible (and more rigorous) to distinguish the two types of system on the basis of the dynamics of their phase transition and the nature of the soft mode involved—propagating or diffusive [14]. Some ferroelectrics and antiferroelectrics, however, defy a strict classification, and fall somewhere in between the displacive and order–disorder types.

2. Experimental procedure

2.1. Synthesis of nanocrystalline $PbZrO_3$

Ultrafine particles of $PbZrO_3$ were synthesized by a modified sol–gel method. An aqueous solution of $Pb(NO_3)_2$ and $ZrOCl_2{\cdot}8H_2O$ was prepared in the required stoichiometric ratio. This solution was poured into NH_4OH solution with the pH being maintained at 10.5 to ensure complete co-precipitation of Pb and Zr as hydroxides. The precipitate was washed with deionized water by repeated decantation so as to bring the pH down to 7. It was then ultrasonicated for 30 min to produce a stable sol. Gelation was done using 2-ethyl hexanol as the dehydrating agent and SPAN-80 as the surfactant. The yellowish brown gel was dried under an infra-red lamp and then heated at 500 °C for two hours to remove any residual carbon. From a thermogravimetric analysis (TGA) of the precursor (dried gel), the formation temperature for $PbZrO_3$ was found to be 650 °C. Different batches of the precursor were heated at different temperatures between 650 °C and 900 °C (for one hour each time) to produce samples with different average particle sizes. 'Bulk' $PbZrO_3$ was obtained by heating the precursor material at 1000 °C for 10 hours. To avoid Pb loss during calcination, all of the samples were heated in an ambient of PbO. This was achieved by placing a mixture of PbO and yttria-stabilized zirconia (1:2 w/w) in a large alumina crucible in which was placed a smaller alumina crucible containing the material to be heated. The pellets and the powder were heated in separate crucibles but at the same time. The larger crucible was covered with an alumina lid.

A Jeol JDX 8030 powder x-ray diffractometer was used for crystallographic phase analysis. Measurements were made with a typical scan speed of 0.3° min^{-1}. All of the samples studied were found by means of x-rays to be single phase. It was also the case that segregated minority phases were not found when the pellets were checked by energy-dispersive x-ray analysis. The lattice constants and the pseudo-tetragonal distortion (c_T/a_T) were calculated using the six most intense diffraction lines in the XRD spectrum.

2.2. Particle size measurement

The particle sizes of the nanocrystalline $PbZrO_3$ samples (after the final heat treatment) were measured by three different techniques. The equivalent spherical diameter (d_{ESD}) of the ensemble of particles was calculated from the surface area analysis technique (the Brunauer–Emmet–Teller method) [15] using a Quantachrome Quantasorb Jr instrument after degassing the samples at 200 °C. The particle size, size distribution, and morphology were examined by a Jeol JSM-840 scanning electron microscope.

The coherently diffracting domain size (d_{XRD}) was calculated from the full width at half-maximum (FWHM) of the (011) diffraction line of $PbZrO_3$ using the well-known Scherrer equation [16]:

$$d_{XRD} = K\lambda/\beta(\theta)\cos\theta \tag{1}$$

where λ is the x-ray wavelength, θ is the angle of diffraction and K is a constant (≈ 1). The FWHM of the diffraction line, $\beta(\theta)$, was corrected for instrumental broadening by subtracting the FWHM of the corresponding line in 'bulk', well-annealed $PbZrO_3$ powder (the reference). If B and b are the measured FWHMs of the diffraction lines (with the same index) in the specimen and the reference sample respectively, then the FWHM of the 'true' diffraction profile is given by

$$\beta(\theta) = B - b^2/B. \tag{2}$$

This equation holds in the comparatively more realistic situation where the line shape cannot be assumed to be either purely Gaussian or purely of Cauchy type [17]. Prior to measuring the FWHM, we eliminated the contribution of the $K\alpha_2$ radiation from the XRD spectra using a modification of the Rachinger method [18].

2.3. Study of the ferroelectric transition

Dielectric measurements were made on pellets with a diameter of 1 cm and thickness of about 0.25 cm. The pellets were obtained by pressing the precursor powder (mixed with a binder, polyvinyl alcohol) and calcining at various temperatures (see section 2.1). Before making the dielectric measurements, the surfaces of the pellets were cleaned in trichloroethylene fumes, and they were coated with air-drying conducting silver paste; this was followed by a baking at 150 °C for one hour. The capacitance and dielectric loss factor were measured at three different frequencies (100 kHz, 500 kHz and 1 MHz) using a HP 4277A impedance analyser. The temperature was measured to an accuracy of ±1 °C using a Pt/Pt–Rh thermocouple. The samples were heated at the rate of 5 °C min^{-1} between room temperature and 150 °C and at 2 °C min^{-1} thereafter. We assumed the ferroelectric-to-paraelectric transition temperature (T_C) to be given by the temperature corresponding to the maximum in the real part of the dielectric response function.

The ferroelectric transition was also studied by differential scanning calorimetry (DSC) in the temperature range 50–350 °C using a Perkin–Elmer DSC-7 power compensation-type calorimeter. The powder samples (≈25 mg) were encapsulated in aluminium crucibles and scanned at the rate of 10 °C min^{-1}.

Table 1. The relation between the equivalent spherical diameter (d_{ESD}) and the coherently diffracting domain size (d_{XRD}) in sol–gel-derived $PbZrO_3$ nanoparticles.

d_{ESD} (nm)	3380	1374	1071	381	286	97
d_{XRD} (nm)	214	130	72	62	36	32
d_{ESD}/d_{XRD}	15.8	10.6	14.8	6.1	7.9	3.0

3. Results and discussion

3.1. Structure and morphology

The particle morphology and size distribution of two representative sol–gel-derived samples (with different average sizes) are shown in the scanning electron micrographs in figures 1(b) and 1(c). Figure 1(a) shows the SEM of a 'bulk' sample (commercial $PbZrO_3$, Johnson–Matthey, 99.997%, heated at 1000 °C for 10 h). Ultrafine $PbZrO_3$ prepared by the sol–gel technique (figures 1(b) and 1(c)) can be seen to possess a reasonably narrow size distribution. As expected, the average particle size obtained from the SEM micrographs compares well with that obtained from the surface area measurements (d_{ESD}). However, d_{XRD} is consistently smaller than d_{ESD} (see table 1) because each particle presumably consists of several coherently diffracting domains; the larger the particle the greater the number of domains that it contains. Since ferroelectric and antiferroelectric phenomena in displacive systems are believed to be controlled by a lattice vibrational mechanism (softening of a TO phonon mode at $\boldsymbol{k} \rightarrow 0$), we expect d_{XRD} to be the dimension most relevant to the present study. In the rest of the paper, the term 'particle size' will, therefore, be assumed to mean d_{XRD}.

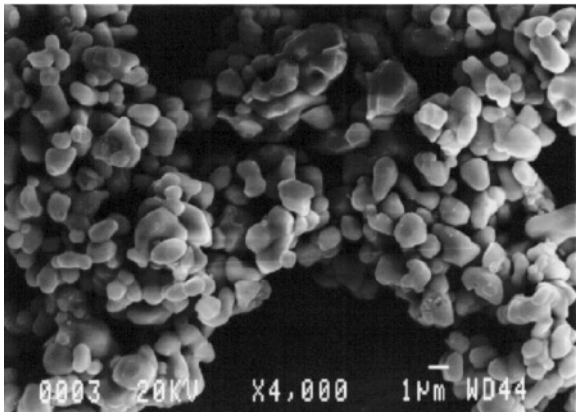

(a)

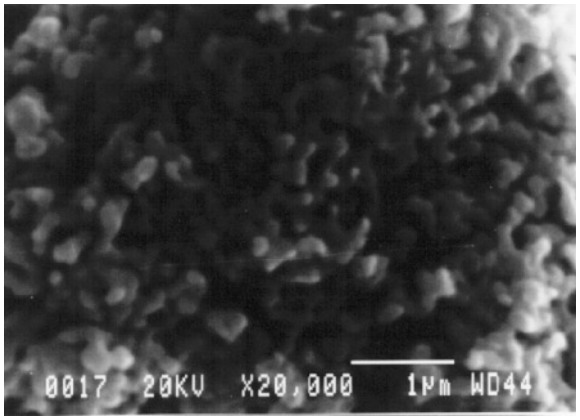

(b)

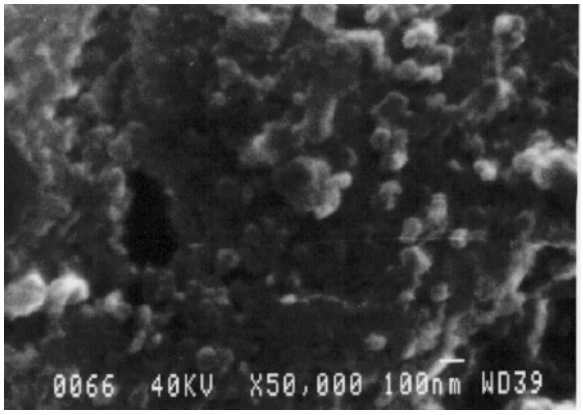

(c)

Figure 1. Scanning electron micrographs of sol–gel-derived $PbZrO_3$ samples with different average sizes: (a) $d_{XRD} = 214$ nm ($d_{ESD} = 3380$ nm), (b) $d_{XRD} = 62$ nm ($d_{ESD} = 381$ nm) and (c) $d_{XRD} = 32$ nm ($d_{ESD} = 97$ nm).

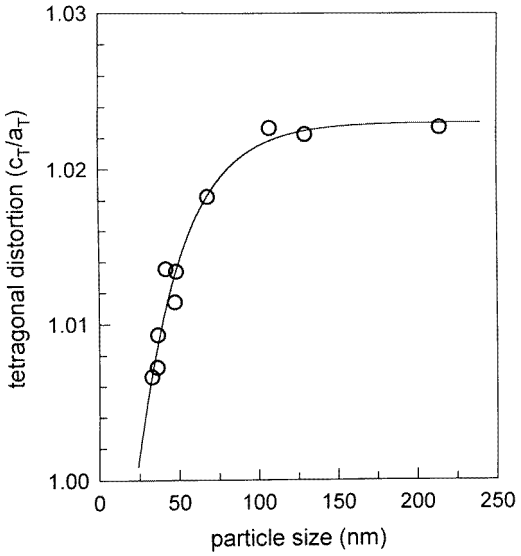

Figure 2. The particle size dependence of the pseudo-tetragonal distortion of the unit cell in $PbZrO_3$, measured at room temperature. The solid line represents a least-squares fit to an empirical function of the form $y \sim 1 - e^{-x}$.

As mentioned in section 1, the paraelectric-to-antiferroelectric transition is accompanied by a pseudo-tetragonal distortion ($c_T/a_T > 1$) of the prototypical cubic unit cell. Figure 2 shows the variation of c_T/a_T with particle size. The crystallographic unit cell remains relatively undistorted down to about 100 nm, below which there is an increasing tendency for it to attain the cubic structure. This behaviour of antiferroelectric $PbZrO_3$ is very similar to that of the ferroelectrics $PbTiO_3$ [10] and $BaTiO_3$ [19]. On least-squares fitting the variation of the tetragonal distortion ($c_T/a_T \equiv y$) with size ($d_{XRD} \equiv x$) to an empirical three-parameter equation of the form

$$y = y_\infty - (y_\infty - 1)\exp[C(d_{crit} - x)] \tag{3}$$

we obtain $d_{crit} = 23(\pm 3)$ nm. Provided an extrapolation of this type is valid, this implies that the crystal structure would become perfectly cubic below a size of 23 nm.

The soft-mode-driven structural distortion in displacive ferroelectrics is an important quantity since it scales with the order parameter: the spontaneous polarization (P_S) or—in the case of antiferroelectrics—the sublattice polarization. This is given by an empirical relation due to Abrahams *et al* [20] of the form $P_S = K\,\Delta z$, where K is a 'universal' constant, and Δz is the saturated value of atomic displacement leading to ferroelectric ordering.

The observed particle size dependence of the crystal symmetry in $PbZrO_3$ is consistent with a general tendency exhibited by a large number of partially covalent oxides. The crystal structure in such systems tends to transform to a higher-symmetry form with decrease in the particle size [21].

3.2. Thermal properties

Figure 3 shows the DSC plots (heat flow versus temperature) of $PbZrO_3$ samples with different particle sizes, where the antiferroelectric phase transition can be seen. T_C is

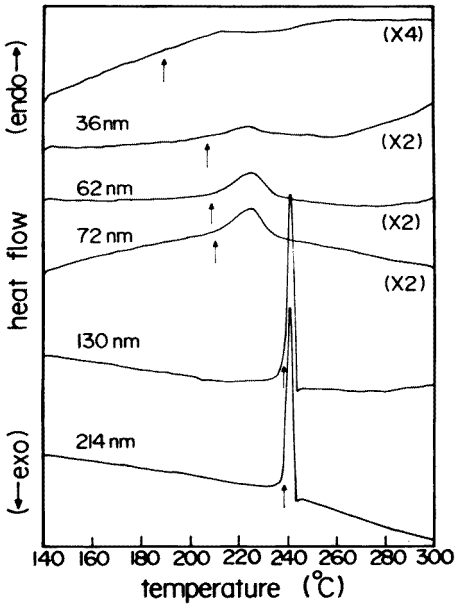

Figure 3. Differential scanning calorimetry data for $PbZrO_3$ particles with different average sizes. All of the measurements were made in the temperature-increasing mode with a scan rate of 10 °C min^{-1}. Arrows indicate the peak onset temperature which is identified with the ferroelectric T_C.

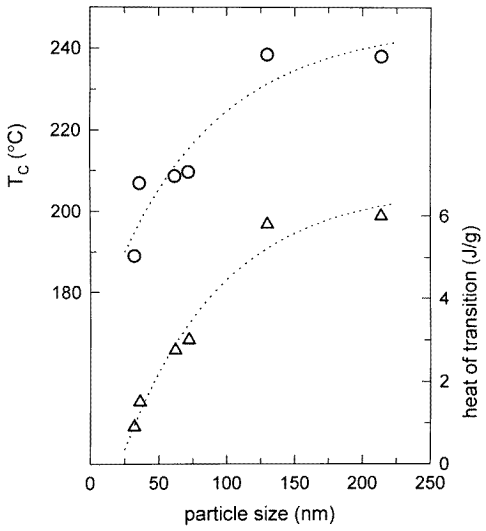

Figure 4. The variation of the ferroelectric T_C (as measured by DSC) and the latent heat of the transition as functions of particle size in $PbZrO_3$. The smooth, dashed line drawn through the data points is merely a visual aid.

conventionally identified with the 'peak onset temperature' (the intersection of the linear portions of the baseline and the leading edge of the peak) in the heat flow versus temperature curve. We see that with a decrease in the particle size below ≈100 nm, the transition becomes progressively broader and the T_C decreases (figure 4). The heat of transition (obtained by integrating the transition peak) is also seen to decrease monotonically with decreasing particle size. For a typical first-order ferroelectric phase transition, the latent heat is given by $\frac{1}{2}T_C\beta P_C^2$, where P_C is the maximum value of the polarization at $T = T_C$ and β is the coefficient of the quadratic term in the free-energy expansion. Since the tetragonal distortion (and hence the sublattice polarization) decreases with reduction in particle size, we expect a smaller latent heat of transition in finer particles. Another contributor to the

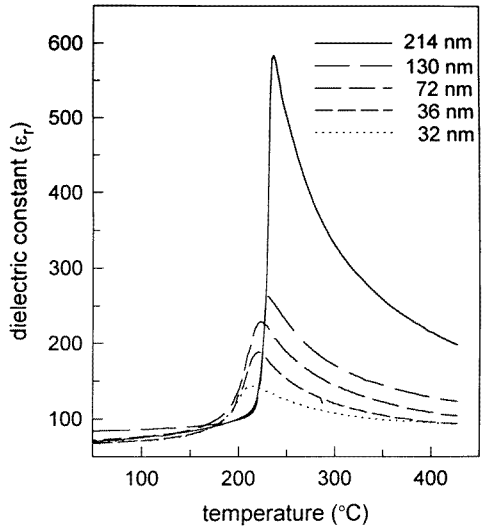

Figure 5. The temperature dependence of the relative dielectric response function (ε_r) for $PbZrO_3$ samples with different average sizes, measured at 500 kHz.

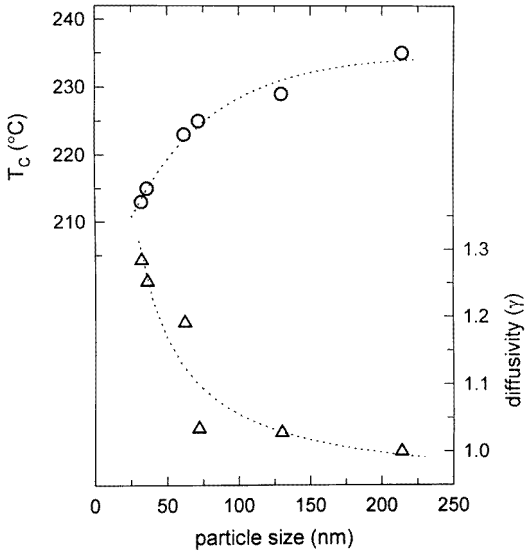

Figure 6. The variation of the ferroelectric T_C (obtained from dielectric measurements) and the diffuseness (γ) as functions of particle size in $PbZrO_3$. The smooth, dashed line drawn through the data points is merely a visual aid.

flattening of the transition peak in smaller particles is the progressive deviation from the ideal Curie–Weiss nature of the phase transition. This aspect is discussed in the next section.

There is an essential difference between the size dependences of the phase transitions in displacive systems such as $PbZrO_3$ and $PbTiO_3$ and order–disorder systems such as $NaNO_2$ [22]. In the latter case, very little change in T_C was observed down to 5 nm, whereas displacive systems start showing deviations in the T_C at sizes as large as 100 nm.

This clearly underscores the importance of the size-induced *structural distortions* in the nanoparticles of the displacive systems. The other obvious difference observed in the two types of system is that the thermal (as well as dielectric) phase transition is not observed at all in nanoparticles of displacive systems with a size below ≈30 nm, while even 5 nm $NaNO_2$ nanoparticles exhibit a clear transition peak.

3.3. Dielectric properties

The temperature dependence of the relative dielectric response function (ε_r) and the dielectric loss factor ($\tan\delta$) were measured between room temperature and 430 °C at different frequencies. Figure 5 shows our results for $PbZrO_3$ samples with different average particle sizes, measured at 500 kHz. With a decrease in the particle size, T_C decreases, ε_{max} decreases, and the peaks become increasingly broader. The monotonic decrease of the dielectric T_C is seen in the plot against particle size in figure 6. The particle size dependences of the antiferroelectric transition in $PbZrO_3$—as observed from the dielectric and the DSC measurements—show qualitatively similar features. The value of $\tan\delta$ remains very low for all of the samples (0.008–0.03) and is not shown.

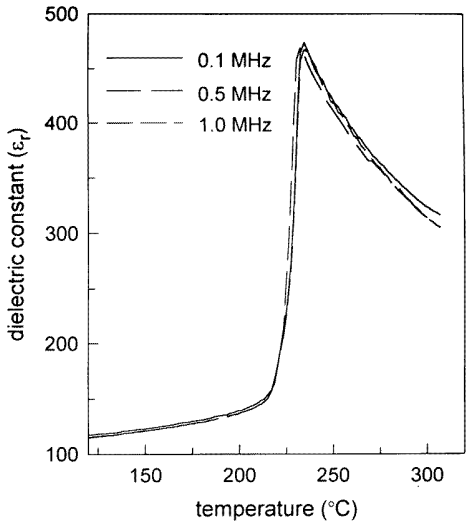

Figure 7. The temperature dependence of ε_r for the $PbZrO_3$ sample with $d_{XRD} = 214$ nm for three different measurement frequencies (100 kHz, 500 kHz, 1 MHz).

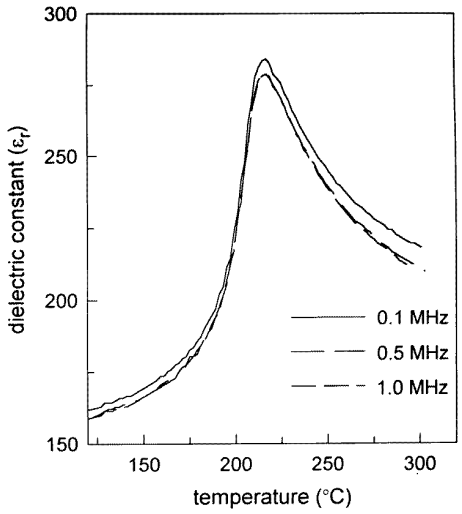

Figure 8. The temperature dependence of ε_r for the $PbZrO_3$ sample with $d_{XRD} = 36$ nm for three different measurement frequencies (100 kHz, 500 kHz, 1 MHz).

Figures 7 and 8 show the frequency variation of the temperature dependence of the dielectric response (real part) for a large-particle (214 nm) and a small-particle (36 nm) sample, respectively. We observe that, unlike for nanocrystalline ferroelectric $PbTiO_3$ [10], T_C and ε_{max} do not show a marked frequency dispersion (between 100 kHz and 1 MHz) in small-sized (36 nm) samples. Dispersion could, however, occur at even smaller sizes.

The dielectric behaviour of nanocrystalline $PbTiO_3$ has been understood on the basis of a *diffuse phase transition* (DPT) model [10]. The 'diffuseness', γ, of a ferroelectric phase transition [23] can be obtained by fitting the high-temperature dielectric data (for $T > T_{max}$, where T_{max} is the temperature corresponding to the peak in the dielectric response) to a

modified Curie–Weiss equation:

$$1/\varepsilon - 1/\varepsilon_{max} = C^{-1}(T - T_{max})^{\gamma}. \quad (4)$$

The critical exponent, γ, is 1 for a conventional Curie–Weiss system, and $\gamma = 2$ for a completely diffuse transition, while $1 < \gamma < 2$ for systems with intermediate degrees of diffuseness. Our data indicate that the diffuseness of the phase transition in nanocrystalline $PbZrO_3$ increases gradually with decreasing size (figure 6).

Diffuse phase transitions were first observed in solid solutions of displacive ferroelectrics of the type $A(P_xQ_{1-x})O_3$. A smearing out of the dielectric response was believed to be due to either local compositional fluctuations (leading to a collection of microscopic regions having a distribution in T_C [24]) or a quenched random disorder which destroys the long-range polar order [25]. The latter may either stabilize the usual domain state (at low concentrations of the dopant species, 'P'), or a dipolar glass state (at higher concentrations of 'P'). Our data on $PbTiO_3$ [10] and $PbZrO_3$ (this paper) show that a diffuse phase transition can occur purely as a particle size effect even in compositionally homogeneous systems with no apparent local atomic disorder.

4. Conclusions

The behaviours of ferroelectric $PbTiO_3$ and antiferroelectric $PbZrO_3$ with decreasing particle size show certain essential similarities. In such displacive-type systems, the soft-mode-driven structural distortion (responsible for stabilizing the ferroelectric or antiferroelectric ordering) decreases monotonically with a reduction in particle size below $\approx$100 nm. This is accompanied by a decrease in the ferroelectric (or antiferroelectric) T_C and the spontaneous polarization. In addition, the paraelectric transition gets increasingly 'smeared out' in smaller particles.

The diffuse phase transition (DPT) in nanoparticles may be explained in terms of either a T_C-distribution model or a dipolar glass model. Unlike in the case of ferroelectric solid solutions (many of which show DPT) in which it is possible to imagine compositionally different islands with different values of T_C, the T_C-distribution in the chemically homogeneous nanoparticle systems could occur essentially as a result of a particle size distribution. Differently sized particles in the same sample would have slightly different values of the ferroelectric distortion (recall that the tetragonality is a strong function of size below $\approx$100 nm) and hence slightly different values of T_C. This would lead to a smeared transition.

A diffuse transition could also occur if the nanoparticulate ferroelectric or antiferroelectric system behaves as a dipolar glass. A dipolar glass is a solid with a regular periodic lattice, some of whose sites are occupied by constituents with a dipole moment which have orientational degrees of freedom [25]. The ferroelectrically 'active' ions which reside at or close to the surface of a nanoparticle would obviously have a totally different coordination from those in the bulk, and the long-range cooperative interactions acting on the former can be expected to vary within certain limits. This could presumably lead to a dipolar glass situation.

We plan to make additional studies of the dielectric relaxational behaviour with the aim of achieving an understanding of the nature of the ferroelectric and antiferroelectric phase transitions in nanoparticles.

Acknowledgment

It is a pleasure to thank Professor Shobo Bhattacharya for several illuminating discussions.

References

[1] Anliker M, Brugger H R and Kanzig W 1954 *Helv. Phys. Acta* **27** 99
[2] Kanzig W 1955 *Phys. Rev.* **98** 549
[3] Martirena T and Burfoot J C 1974 *J. Phys. C: Solid State Phys.* **7** 3182
[4] Srinivasan M R, Multani M S, Ayyub P and Vijayraghavan R 1983 *Ferroelectrics* **51** 137
[5] Francombe M H 1993 *Physics of Thin Films: Mechanical and Dielectric Properties* ed M H Francombe and J L Vossen (San Diego, CA: Academic) pp 225–300
[6] Zhong W L, Wang Y G, Zhang P L and Qu B D 1994 *Phys. Rev.* B **50** 698
[7] Zhong W L, Jiang B, Zhang P L, Ma J M, Cheng H M, Yang Z H and Li L X 1993 *J. Phys.: Condens. Matter* **5** 2619
[8] Ishikawa K, Yoshikawa K and Okada N 1988 *Phys. Rev.* B **37** 5852
[9] Uchino K, Sadanaga E and Hirose T 1989 *J. Am. Ceram. Soc.* **72** 1555
[10] Chattopadhyay S, Ayyub P, Palkar V R and Multani M 1995 *Phys. Rev.* B **52** 13 177
[11] Okazaki K and Nagata K 1973 *J. Am. Ceram. Soc.* **56** 82
[12] Arlt G, Hennings D and de With G 1985 *J. Appl. Phys.* **58** 1619
[13] Dai X, Li J-F and Viehland D 1995 *Phys. Rev.* B **51** 2651
[14] Lines M E and Glass A M 1977 *Principles and Applications of Ferroelectrics and Related Materials* (Oxford: Clarendon) p 10
[15] Allen T 1975 *Particle Size Measurement* (London: Chapman and Hall) p 358
[16] Wilson A J C 1962 *Proc. Phys. Soc.* **80** 286
[17] Anantharaman T R and Christian J W 1956 *Acta Crystallogr.* **9** 479
[18] Rachinger W A 1948 *J. Sci. Instrum.* **25** 254
[19] Schlag S, Eicke H-F and Stern W B 1995 *Ferroelectrics* **173** 351
[20] Abrahams S C, Kurtz S K and Jamieson P B 1968 *Phys. Rev.* **172** 551
[21] Ayyub P, Palkar V R, Chattopadhyay S and Multani M S 1995 *Phys. Rev.* B **51** 6135
[22] Marquardt P and Gleiter H 1982 *Phys. Rev. Lett.* **48** 1423
[23] Uchino K and Nomura S 1982 *Ferroelectr. Lett.* **44** 55
[24] Cross L E 1987 *Ferroelectrics* **76** 241
[25] Höchli U T, Knorr K and Loidl A 1990 *Adv. Phys.* **39** 405